

The imprint of presupernova evolution on supernovae remnants

Carles Badenes

badenes@ieec.fcr.es

and

Eduardo Bravo

eduardo.bravo@upc.es

Dept Física i Enginyeria Nuclear, Universitat Politècnica de Catalunya, Av Diagonal 647,
08028 Barcelona, and

Institut d'Estudis Espacials de Catalunya, Edifici Nexus, Gran Capità 2, 08034 Barcelona,
Spain

Received _____; accepted _____

Submitted to: ApJVersion: December 24, 2018

ABSTRACT

The evolution of type Ia supernova binary system progenitors is highly uncertain. Several evolutionary models predict that the accretion of mass onto the white dwarf is accompanied by mass ejection from the binary in the form of a powerful wind, but very few observations have been made during the initial phase of formation of supernovae remnants, when the interaction of supernova ejecta with presupernova wind could be tested. Here we present hydrodynamical simulations of supernova ejecta interaction with an ambient medium modified by presupernova wind. The structure of the ambient medium when the supernova explodes is very sensitive to the details of wind history, and the evolution of the supernova remnant can be affected during several thousand years. We have found that the forward shock expansion parameter is a good tool for discriminating between several wind models. The evolution of the supernova remnant in the presence of an ambient medium modified by interaction with pre-supernova wind cannot be described by a similarity solution. We also rule out simple models based on a circumstellar medium that merges smoothly with a uniform density ambient medium.

Subject headings: binaries: close — circumstellar matter — stars: evolution — supernovae: general — stars: winds, outflows — ISM: supernova remnants

1. Introduction

The evolution of type Ia supernova (SNIa) binary system progenitors is highly uncertain. Although there is consensus that the exploding star is a white dwarf made of carbon and oxygen, the nature of the companion star, the observational counterpart of

the binary, and the detailed evolutionary phases of the system prior to SN explosion are currently the matter of strong debate (see, for instance, Canal, Méndez, & Ruiz-Lapuente 2001, and references therein). Those uncertainties raise doubts about the use of high-redshift SNIa for cosmological purposes, especially as their calibration is only based on the properties of local SNIa. One way to discern among the various presupernova models is to look for their consequences on supernova remnant evolution.

Models of supernovae remnants (SNR) originated by a SNIa usually assume either a uniform density interstellar medium (ISM) or a $\rho \propto r^{-2}$ circumstellar medium (CSM), produced by a constant mass loss rate wind (Dwarkadas & Chevalier 1998, for instance). This assumption, together with an appropriate choice of the SN ejecta profile, allows for the existence of similarity solutions that describe the early evolution of the SNR (Chevalier 1982; Truelove & McKee 1999). Detailed models of pre-SNIa binary system evolution, however, point to a time varying mass loss rate (Hachisu, Kato, & Nomoto 1996; Langer et al. 2000), which is expected to lead to ambient medium (AM) density profiles very different from a power law.

Very few observations have been made during the initial phase of formation of supernovae remnants, when the interaction of supernova ejecta with presupernova wind could be tested. Schlegel & Petre (1993) used ROSAT to search for X-ray emission from the type Ia SN1992A 16 days after visual maximum, and derived an upper limit for the presupernova mass-loss rate of less than a few times $10^{-6} M_{\odot} \text{yr}^{-1}$. Cumming et al. (1996) looked for narrow $H\alpha$ in a high-resolution spectrum of SN1994D, another SNIa, and derived an upper limit for the mass loss rate of $\sim 1.5 \times 10^{-5} M_{\odot} \text{yr}^{-1}$. These observations have in common that they were made at a very early phase in the supernova ejecta evolution, implying that they only probed the CSM very close to the progenitor. The AM region up to a few parsecs can be probed by the evolution of young SNR.

Here we present hydrodynamical simulations of supernova ejecta interaction with an AM modified by presupernova wind. We have worked out simple models of time dependent wind, devised to reproduce the history of wind given by pre-SNIa binary system evolutionary models. The main results of the simulations are presented and the compatibility of each wind model with known SNR from SNIa is discussed, based on the different outcomes of the calculations (mainly, expansion parameters, velocity of the ejecta at the reverse shock, and radius of the SNR).

2. Hydrodynamical simulations of wind interaction with ambient medium and SN ejecta

2.1. Wind models

Current models of presupernova binary evolution describe wind ejection as a subproduct of matter accretion on the primary star, once it has become a white dwarf. In the last years, there has been a wide interest on the possibility (Hachisu, Kato, & Nomoto 1996) that an optically thick wind stabilizes the mass transfer in the binary system, thus opening a new channel for the white dwarf to grow up to the Chandrasekhar mass and explode as a SNIa (Li & van den Heuvel 1997; King & van Teeseling 1998; Hachisu, Kato, & Nomoto 1999). The time history of wind is complex, and depends on orbital parameters as well as on the capability of the white dwarf to quietly accrete the matter transferred from the secondary star. An important characteristic of the wind history is whether the wind is active up to the time of SN explosion or, on the contrary, the binary has a time extended phase of conservative evolution prior to white dwarf ignition. Another important parameter is the velocity of the wind. Here we explore the effects of the wind on the SNR evolution, and compare with the results obtained on the assumption that there is no significant presupernova wind.

We have worked out simple models of time dependent wind, devised to reproduce the gross features of the wind history predicted by binary system evolutionary models. In all our wind models the rate at which mass is lost by the binary system as a wind, \dot{M}_w , has a linear time dependence: $\dot{M}_w = a - bt$, with a , b two positive parameters, and the wind velocity, v_w , remains constant with time. The wind can either be active until the moment of supernova explosion, as in models C (fast wind) and D (slow wind), or it can decrease to zero, leaving the system in a phase in which there is no wind ejection until the explosion ensues, as in models A (fast wind) and B (slow wind). The parameters for the models are given in table 1 and figure 1.

2.2. Wind interaction

We have studied the hydrodynamical processes induced by the wind ejection: first, its interaction with the AM and, second, the formation and evolution of the SNR. The simulations were performed with a standard one dimensional hydrodynamical code similar to that described in Truelove & McKee (1999), with the equations modified to include a source of mass and momentum at the center, to simulate wind ejection. The ISM density was set to 10^{-24} g cm $^{-3}$ in all cases.

The resulting AM density profiles at the time of SN explosion are shown in figure 2. The interaction of the wind ejected by the progenitor system and the surrounding ISM follows a mechanism very similar to that at work in SNR: high speed ejecta flow into a uniform, stationary medium and push it away resulting in a doubly-shocked structure with a contact discontinuity between the wind and the ISM. A forward shock (prominent in all the profiles shown in figure 2) propagates into the ISM, heating, compressing and accelerating it, while a reverse shock propagates inward, heating, compressing and decelerating the inner wind material. The kinetic energies involved, however, are four to seven orders of

magnitude lower than those characteristic of SN explosions, and therefore the involved shock velocities and temperatures are far below those typically found in SNR. This kind of interaction between the wind and the ISM is not expected to produce significant observational counterparts given the density and temperature ranges involved.

The models with the highest wind velocity (A and C) produce a very large bubble of low density AM around the SN. Model C presents the largest bubble, because the time elapsed between the beginning of the wind and SN explosion is the largest of the four models. One should expect this feature to have a major impact on the evolution of the young SNR, delaying the formation of the radiation emitting structures of the remnant. Model D (low velocity wind) is the only one in which a power law structure can be identified close to the center. In this model, the reverse shock formed by the interaction of the wind with the ISM lies at a radius of 3 pc, being the only model in which the reverse shock has not reached the center at the time of SN explosion. Model B, characterized by a low velocity wind with a high mass loss rate, does not show a circumstellar region near to the center because the wind stops blowing long before SN explosion. This model presents the smoother density structure, broken only by the presence of a contact discontinuity.

Once the SN explodes, and after the SNR characteristic doubly-shocked structure is formed, the forward shock propagation, and therefore the whole dynamical evolution of the SNR (shock velocities, expansion parameters, etc.) will depend on the AM density gradient encountered. We have performed hydrodynamical simulations of SNR evolution assuming an exponential model for the SN ejecta density profile (Dwarkadas & Chevalier 1998), with a total mass $1.4 M_{\odot}$ and a kinetic energy $K = 0.98 \times 10^{51}$ erg, and with the AM structures obtained previously for the four wind models.

In figure 3 we show the density profile at the age of Tycho’s SNR for wind model A (other wind models look similar, although details vary from case to case, especially the

time scale), together with the SNR obtained for the same exponential SN ejecta evolving into a constant density AM (i.e. with no wind, henceforth EXPNW). The influence of the wind on the SNR is clearly seen: the location of the doubly-shocked structure is farther away (and, for model A, clearly inconsistent with Tycho’s SNR) and its density is two orders of magnitude lower than in the EXPNW model. We stress that the structures that appear outside the region delimited by the forward and the reverse shocks would remain undetectable due to the low temperatures involved.

The evolution of the SNR in presence of the AM modified by the wind is far from being self-similar. For instance, once the forward shock runs into the contact discontinuity between the wind and the ISM, it will experience a dramatic change of behavior due to the strong positive density gradient. Another change should be expected when the SNR forward shock runs into the wind forward shock. We emphasize that, depending on the wind model adopted, these interactions can occur very early in the evolution of the SNR.

3. Discussion and conclusions

We now proceed to analyze the implications of the computed hydrodynamical evolutions on the observational properties of SNRs. We will concentrate on a few relevant characteristics of SNRs: expansion parameters, velocity at the reverse shock, and radius of the forward shock.

Figure 4a shows the temporal evolution of the expansion parameter of the SNR forward shock, which reflects the complexity of the AM structure found by the SN ejecta. It is evident that the interaction of the wind with the ISM influences the evolution of the SNR during several thousands of years. At the end of the simulations ($\sim 4 \times 10^{10}$ s after SN explosion) only model EXPNW and wind model B are close to the Sedov phase (forward

shock expansion parameter $\eta_f = 0.4$). The evolution of wind models A and D is similar: they experience a phase of rapid expansion, with values of η_f comparable to the EXPNW model, until the forward shock reaches the end of the low-density bubble, which causes the shock to slow down. There follows a long phase in which $\eta_f = 0.2 - 0.3$ remains nearly constant with slight speed ups. The passage of the SNR forward shock through the wind-AM contact discontinuity produces a reflected component that rebounds at the ejecta-wind contact discontinuity and overcomes the forward shock itself at $t \sim 2.3 \times 10^{10}$ s in models A and D, producing the first speed ups. The speed up at $t \sim 3 \times 10^{10}$ s (model D) is produced when the SNR forward shock overcomes the wind forward shock (this feature is out of the figure time range for model A). The speed up experienced by model B at $t \sim 1.8 \times 10^{10}$ s is also due to the coalescence of the forward shock of the SNR with that due to the interaction of the wind with the ISM. The simulation corresponding to model C was ended when the SNR forward shock arrived to the end of the low-density bubble, due to the strong density contrast found there.

Figure 4b shows the temporal evolution of the expansion parameter of the SNR reverse shock. As with the forward shock, in the wind models there are several secondary, transmitted and reflected, shock waves that affect the evolution of the SNR reverse shock, a feature that is not present in model EXPNW and that is less evident in wind model B, due to the relative smoothness of its density profile. The sudden decrease of the expansion parameter found in models A and D is caused by the arrival of the secondary shock wave generated when the forward shock reaches the end of the low-density bubble. Starting from the forward shock slow down discussed earlier, this reflected wave travels rapidly down the negative density gradient of shocked wind, overcomes the ejecta-wind contact discontinuity and, finally, coalesces with the SNR reverse shock, giving it a push that drives η_r into negative values.

The location of the reverse shock in lagrangian coordinate is better seen in figure 5a, where the velocity of the SN ejecta just ahead of the innermost shock is shown and compared to the EXPNW model. The presence of low-density bubbles in all wind models has two consequences. First, the build-up of the SNR shocks is delayed, because the matter found by the expanding SN ejecta is so thin that it takes a lot more time to influence the hydrodynamic evolution of the ejecta. This causes a delay in the penetration of the SNR reverse shock into the SN ejecta (and, therefore a larger velocity compared to the EXPNW model at the same epoch). Second, when the SNR reverse shock has already been created, the density of SN ejecta that it encounters is lower in the wind models, due to the longer expansion time. This results in a more efficient inwards propagation of the reverse shock, which finally converges with that of the EXPNW model. In this figure, a change of the behavior of the SNR reverse shock in models A and D can also be seen, which is due to the coalescence of this shock and the one reflected in the density barrier found at the end of the low-density bubble that we have already mentioned.

Although we have made no attempt to fit the parameters of the wind models to reproduce the properties of any particular SNR, the comparison of our results with the well known SNR from Tycho’s SN and SN1006 can be instructive. When comparing our models to real SNRs, it should be kept in mind that the details of the wind and SNR evolution depend on the precise value chosen for the ISM density at the beginning of the simulations (for instance, a value of the ISM density lower than we have chosen would result in a larger low-density bubble and, thus, in a longer phase of high expansion parameter, but also in larger velocities at the reverse shock and larger radius of the SNR).

The average expansion parameter of Tycho’s SNR has been determined in radio and visible wavelengths to be in the range 0.4 – 0.5. Hughes (2000) used *ROSAT* X-ray data fitted to analytic models of Truelove & McKee (1999) to obtain $\eta_f = 0.64$ and $\eta_r = 0.49$.

While the reverse shock expansion parameter is not particularly constraining with respect to the different wind models, the high value found by Hughes (2000) for the forward shock expansion parameter can only be reproduced by wind models A and C (i.e., those with the largest bubble) and, marginally, by the EXPNW model (we note that Hughes found that his data could only be fitted by a model based on a uniform density ejecta, but such a SN model is not realistic). However, inspection of figure 5b shows that Tycho’s SNR radius is indeed too small when compared to models A and C. A decrease in the initial value of the ISM density would lead to a larger expansion parameter but also to a larger SNR radius. A spectral analysis of X-ray data does also pose constraints on the state of the SNR. Dwarkadas & Chevalier (1998) suggested the existence of a CSM with $\rho \propto r^{-2}$ up to 0.67 pc from the center merging smoothly into a uniform density AM, in order to explain the spectroscopic features produced by Si, S and Fe. However, such a smooth structure is in fact ruled out by our simulations of interaction of the wind with the ISM.

With respect to SNR1006, the X-ray data point to a forward shock expansion parameter $\eta_f = 0.5$, and a velocity of the SN ejecta ahead of the reverse shock of the order of $v = 4500 - 6300 \text{ km s}^{-1}$. Measurements in the visible range give a lower η_f of 0.33 (Long, Blair & van den Bergh 1988). The only model compatible with the large value of v is wind model A, which also gives a reasonable size for SNR1006. On the other hand, wind model A is marginally compatible with the expansion parameter found in the visible. One intriguing feature of SNR1006 is the acceleration of cosmic rays up to the TeV energy range. We suggest the possibility that the presence and interaction of several secondary shock waves, due to a low-density bubble produced by a wind could be relevant to the explanation of the mechanism of acceleration of cosmic rays in SNRs.

To conclude, we have shown that the wind ejected by the progenitor system of a SNIa has a dramatic influence on the evolution of the corresponding SNR, which is not

correctly represented by the current assumption of a CSM described by a simple power law and smoothly continued by a uniform density AM. If current models of pre-SNIa binary evolution are correct, the early evolution of their SNR cannot be described by any kind of similarity solution. On the other hand, a few restrictions can also be put on presupernova evolution. None of the wind models explored here is compatible with the known properties of Tycho's SNR, whereas wind model A (characterized by a high velocity wind lasting for about 2×10^5 yr, followed by a phase of conservative evolution) gives results consistent with several features of SNR1006. It is clear that a more complete exploration of the space of parameters describing pre-supernova wind is of high interest.

This work has been supported by the MCYT grants ESP98-1348 and AYA2000-1785, and by the DGES grant PB98-1183-C03-02. CB is very indebted for a CIRIT grant.

REFERENCES

- Canal, R., Méndez, J., & Ruiz-Lapuente, P. 2001, *ApJ*, 550, L53
- Chevalier, R. A. 1982, *ApJ*, 258, 790
- Cumming, R. J., Lundqvist, P., Smith, L. J., Pettini, M., & King, D. L. 1996, *MNRAS*, 283, 1355
- Dwarkadas, V. V., & Chevalier, R. A. 1998, *ApJ*, 497, 807
- Hachisu, I., Kato, M., & Nomoto, K. 1996, *ApJ*, 470, L97
- Hachisu, I., Kato, M., & Nomoto, K. 1999, *ApJ*, 522, 487
- Hughes, J. P. 2000, *ApJ*, 545, L53
- King, A. R., & van Teeseling, A. 1998, *A&A*, 338, 965
- Li, X. D., & van den Heuvel, E. P. J. 1997, *A&A*, 322, L9
- Langer, N., Deutschmann, A., Wellstein, S., & Höfflich, P. 2000, *A&A*, 362, 1046
- Long, K. S., Blair, W. P., & van den Bergh, S. 1988, *ApJ*, 333, 749
- Schlegel, E. M., & Petre, R. 1993, *ApJ*, 412, L29
- Truelove, J. K., & McKee, C. F. 1999, *ApJS*, 120, 299

Table 1. Parameters of wind models A, B, C, D

| a | b | t_{end} | t_{SN} | v_{w} | M_{w} | K_{51} |
|-----|------|------------------|-----------------|----------------|----------------|---------------------|
| 2 | 10 | 0.2 | 0.7 | 200 | 0.2 | $8 \cdot 10^{-5}$ |
| 2 | 10 | 0.2 | 0.7 | 20 | 0.2 | $8 \cdot 10^{-7}$ |
| 0.6 | 0.27 | 1.5 | 1.5 | 200 | 0.6 | $2.4 \cdot 10^{-4}$ |
| 0.6 | 0.27 | 1.5 | 1.5 | 20 | 0.6 | $2.4 \cdot 10^{-6}$ |

Note. — Units of a and b are $10^{-6}M_{\odot}\text{yr}^{-1}$ and $10^{-12}M_{\odot}\text{yr}^{-2}$, respectively, t_{end} is the duration of the wind phase and t_{SN} is the time of the SN explosion, both in Myr, v_{w} is the wind velocity, in km/s, M_{w} is the total mass ejected in the wind, in M_{\odot} , K_{51} is the total kinetic energy of the wind, in 10^{51} erg

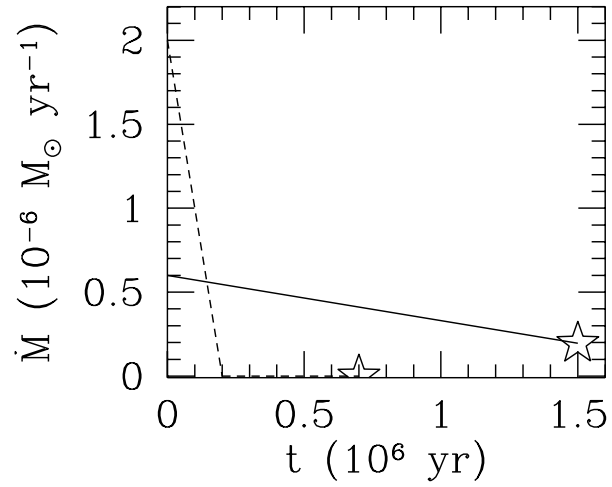


Fig. 1.— Time evolution of wind mass loss rate for models A and B (dashed line) and models C and D (solid line). The time at which the SN explodes is identified by a \star . Models A and B are characterized by a phase of conservative binary evolution prior to SN explosion

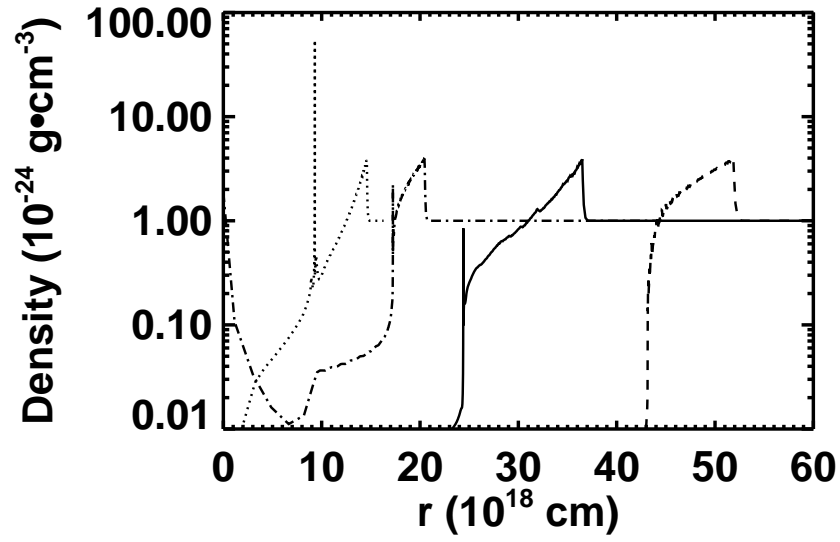


Fig. 2.— Results of the hydrodynamical simulations: AM density profile at the time of SN explosion for the four wind models. Lines correspond to wind models A (solid), B (dotted), C (dashed), and D (dash-dotted)

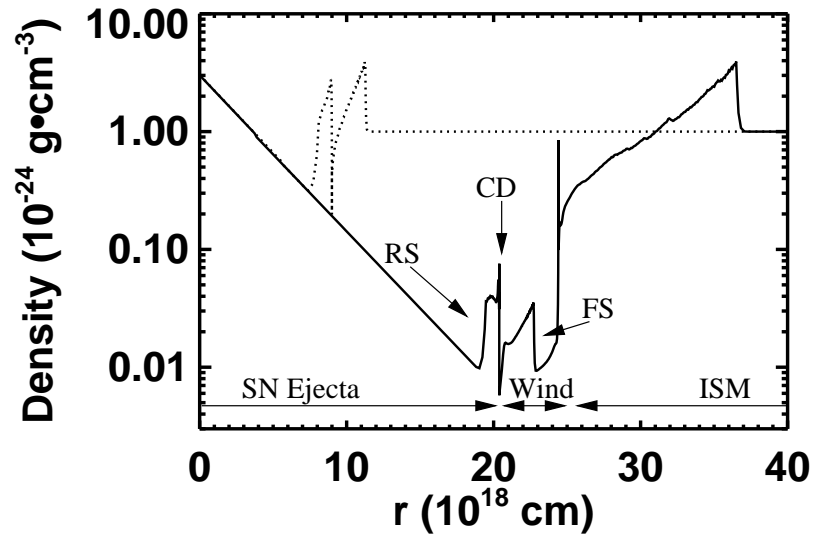


Fig. 3.— Results of the hydrodynamical simulations of SNR evolution at the age of Tycho’s SNR. The SN ejecta was modelled by an exponential density profile, and the wind by model A (solid line). Model EXPNW is also shown (dotted line). Labels RS, CD, and FS mark the positions of the reverse shock, the contact discontinuity, and the forward shock

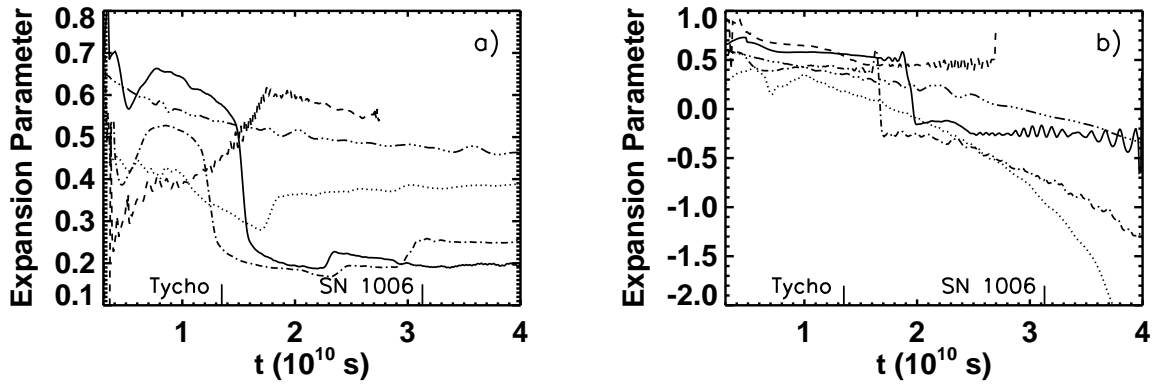


Fig. 4.— Expansion parameter of the forward shock (a) and the reverse shock (b) as a function of time. The ages of Tycho’s SNR and SNR 1006 are marked above the horizontal axis. Lines correspond to wind models A (solid), B (dotted), C (dashed), D (dash-dotted), and model EXPNW (dash-dot-dot-dotted)

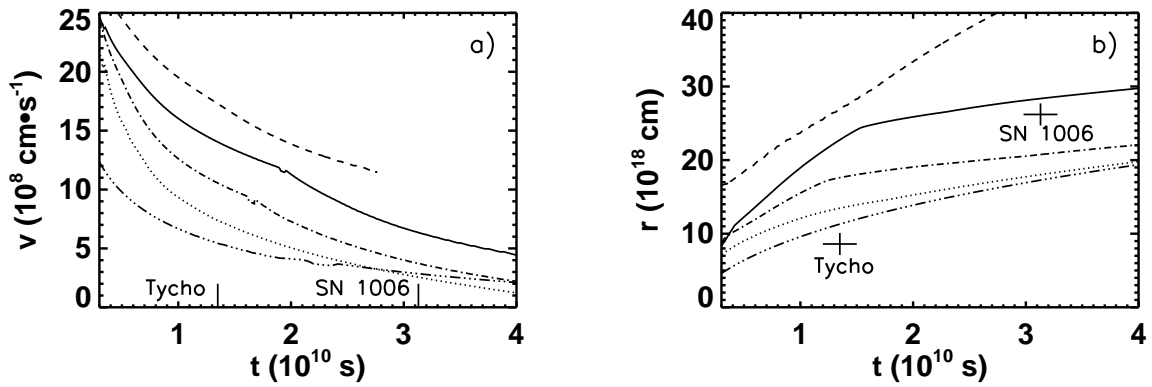


Fig. 5.— Expansion velocity at the reverse shock (a) and radius of the forward shock (b) as a function of time. The ages of Tycho’s SNR and SNR 1006 are marked above the horizontal axis. Lines correspond to wind models A (solid), B (dotted), C (dashed), D (dash-dotted), and model EXPNW (dash-dot-dot-dotted)